Supporting Information

Theoretical Studies on Full-Color Thermally Activated Delayed Fluorescence Molecules

Lei Liu,[a] Qi Wei ,[a] Yajuan Cheng, [b] Huili Ma,*[c] Shiyun Xiong,*[a] Xiaohong Zhang,*[a]

a.Institute of Functional Nano & Soft Materials (FUNSOM), Jiangsu Key Laboratory for Carbon- Based Functional Materials & Devices, Soochow University, Suzhou, 215123, Jiangsu ,P.R. China.
*E-mail: xiongshiyun216@163.com; xiaohong_zhang@suda.edu.cn
b.Key Laboratory of Organic Synthesis of Jiangsu Province and the State and Local Joint Engineering Laboratory for Novel Functional Polymeric Materials, College of Chemistry, Chemical Engineering and Materials Science, Soochow University, Suzhou 215123, P. R. China.
c.Key Laboratory of Flexible Electronics (KLOFE) & Institute of Advanced Materials (IAM), Nanjing Tech University (NanjingTech), 30 South Puzhu Road, Nanjing 211816, P. R. China. *E-mail: iamhlma@njtech.edu.cn

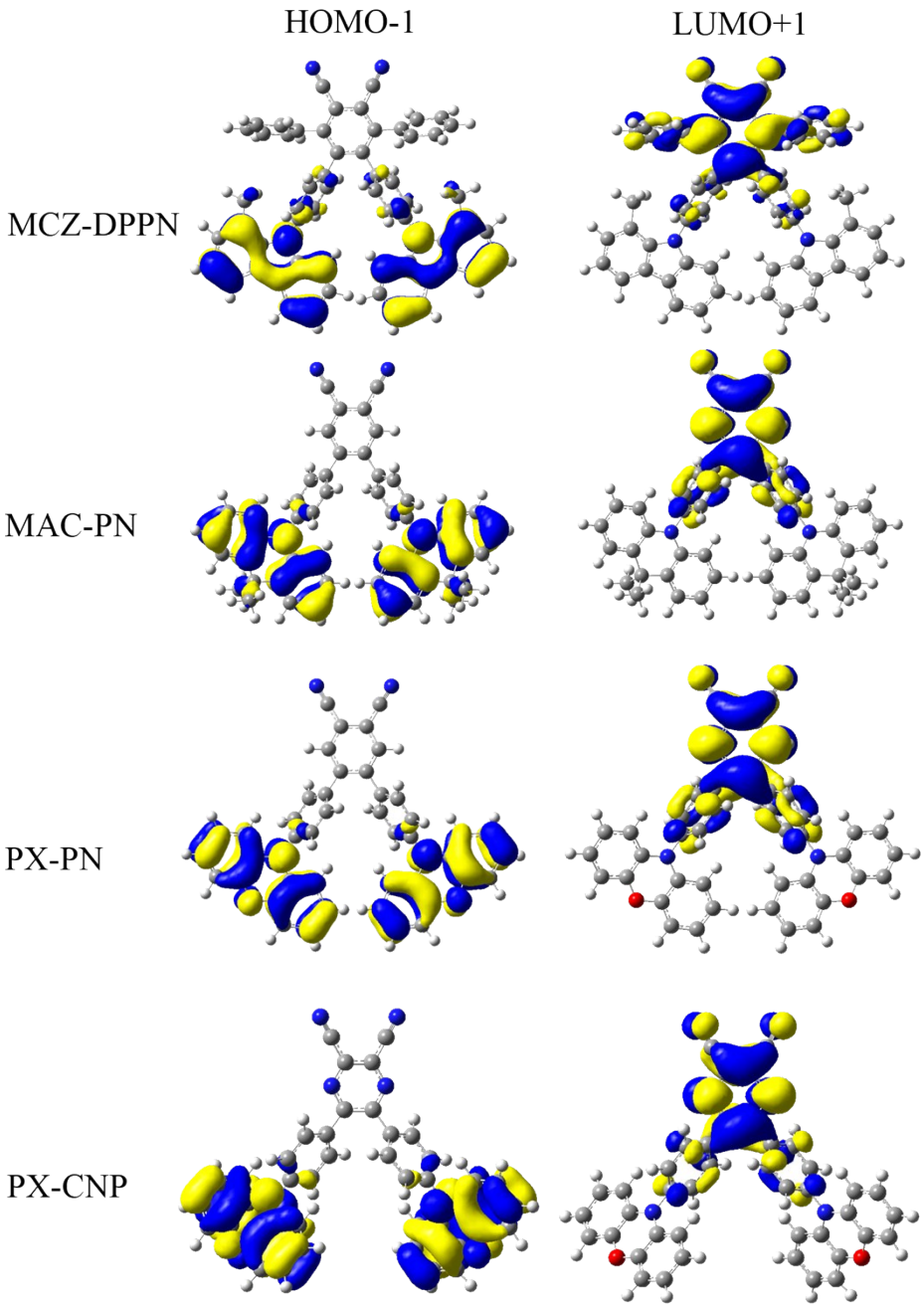

Figure S1. The orbital distributions of the investigated molecules for HOMO-1 and LUMO + 1.

The total reorganization energy can be further decomposed on each vibrational mode based on the harmonic oscillator approximation as follows:

$$\lambda_k = \sum \lambda_i = \sum h\omega_i S_i ; S_i = \frac{\omega_i D_i^2}{2\hbar} \quad (1)$$

Where ω_i and S_i represent the frequency of the i-th normal mode and the Huang-Rhys factor, and D_i is the displacement along the i-th normal mode coordinate between the equilibrium

positions of the two electronic states. The Huang-Rhys factor and reorganization energy for each normal mode are useful parameters for estimating the degree of electron-vibration coupling between different states.

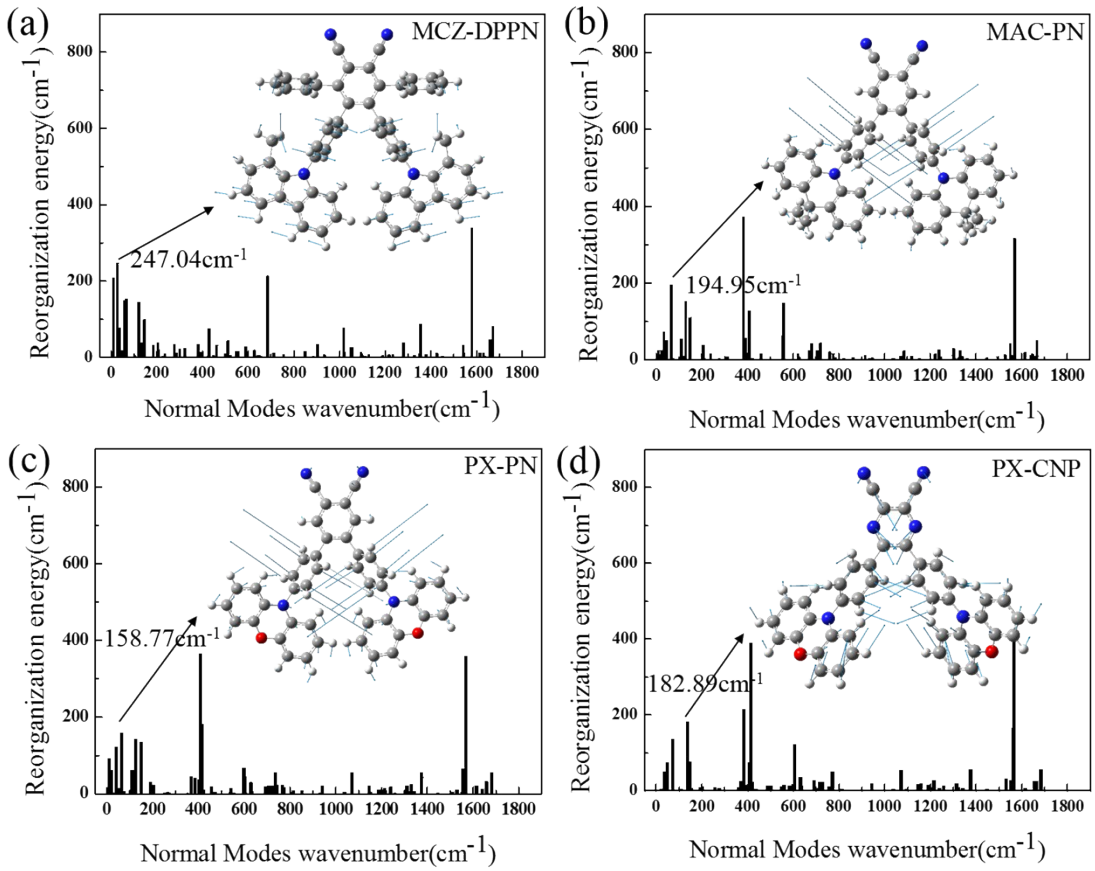

Figure S2. The reorganization energies for the S_0 state in the S_0-S_1 transition versus the normal mode frequencies. Representative vibration modes are shown in the insets.

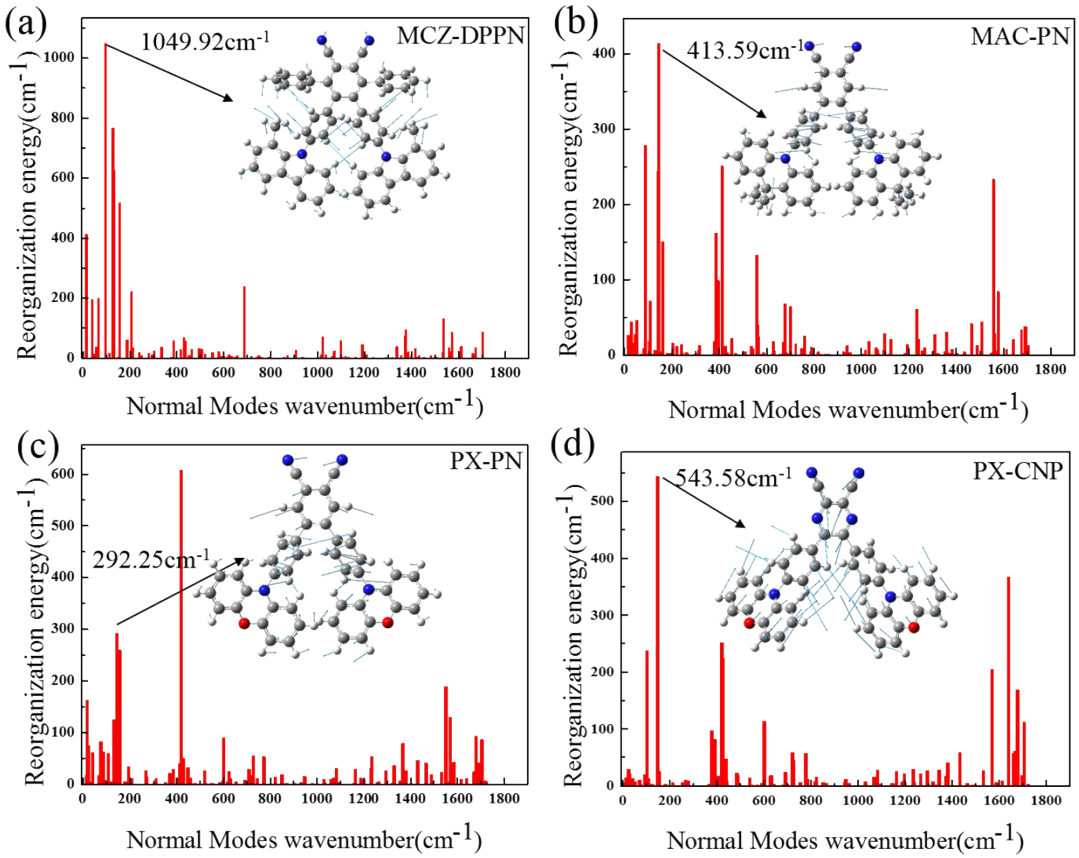

Figure S3. The reorganization energies for the S_1 state in the S_0-S_1 transition versus the normal mode frequencies. Representative vibration modes are shown in the insets.

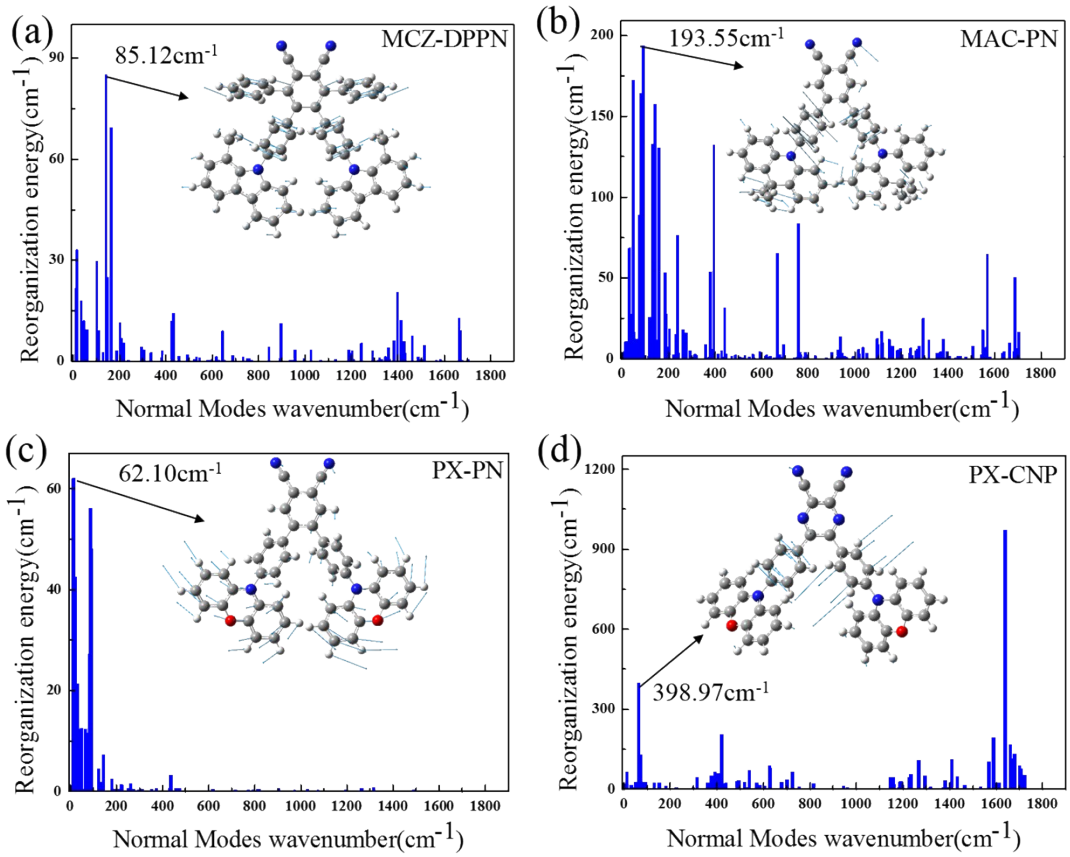

Figure S4. The reorganization energies for the T_1 state in the S_1-T_1 transition versus the normal mode frequencies. Representative vibration modes are shown in the insets.

Table S1. Hartree-Fock percentage (HF%) of different functionals, the adiabatic absorption ($\lambda_{abs}(S_1)$) and emission wavelength ($\lambda_{emi}(S_1)$) calculated by different functionals (with the unit of nm). Vertical transition energy of S_1 ($E_{vert}(S_1)$) and T_1 ($E_{vert}(T_1)$) as well as their vertical energy gap ($\Delta E_{ST}(vert)$) and energy gap ($\Delta E_{ST}(exp)$) in experiment (with the unit of eV).

		HF%	λ_{abs} (S_1)	λ_{emi} (S_1)	E_{vert} (S_1)	E_{vert} (T_1)	ΔE_{ST} $(vert)$	ΔE_{ST} (exp)
MAC-DPPN	B3LYP*	15%	484	593	2.5689	2.5572	0.0117	0.36
	B3LYP	20%	441	532	2.8117	2.7879	0.0238	
	PBE0	25%	407	474	3.0446	2.8783	0.1663	
	MPW1B95	31%	378	442	3.2847	3.1281	0.1566	
	BMK	42%	331	410	3.7417	3.2771	0.4646	
	M062X	54%	299	391	4.1440	3.5317	0.6123	
	M06HF	100%	263	371	4.7109	3.9748	0.7361	
MAC-PN	B3LYP*	15%	625	712	1.9841	1.9815	0.0026	0.20
	B3LYP	20%	557	623	2.2269	2.2234	0.0035	
	PBE0	25%	508	574	2.4415	2.4349	0.0066	
	MPW1B95	31%	462	543	2.6837	2.6764	0.0073	
	BMK	42%	396	449	3.1302	3.0890	0.0412	
	M062X	54%	350	408	3.5381	3.3650	0.1731	
	M06HF	100%	276	336	4.4894	3.8036	0.6858	
PX-PN	B3LYP*	15%	718	860	1.7268	1.7210	0.0058	0.08
	B3LYP	20%	628	732	1.9759	1.9686	0.0073	
	PBE0	25%	565	661	2.1942	2.1821	0.0121	
	MPW1B95	31%	508	616	2.4417	2.4283	0.0134	
	BMK	42%	430	507	2.8820	2.8496	0.0324	
	M062X	54%	376	440	3.2980	3.2253	0.0727	
	M06HF	100%	288	348	4.3065	3.6286	0.6779	
PX-CNP	B3LYP*	15%	979	1238	1.2666	1.2557	0.0109	0.04
	B3LYP	20%	823	996	1.5068	1.4954	0.0114	
	PBE0	25%	722	889	1.7179	1.7032	0.0147	
	MPW1B95	31%	635	808	1.9538	1.9393	0.0145	
	BMK	42%	525	624	2.3598	2.3375	0.0223	
	M062X	54%	444	512	2.7960	2.7567	0.0393	
	M06HF	100%	317	365	3.9062	3.3883	0.5179	

Table S2. Calculated charge transfer (CT) and local excitation (LE) characters for the S_1 and T_1 states of the investigated molecules.

	S_1		T_1	
	CT	LE	CT	LE
MAC-DPPN	81.77%	18.23%	71.76%	28.24%
MAC-PN	88.75%	11.25%	88.12%	11.88%
PX-PN	89.74%	10.26%	88.77%	11.23%
PX-CNP	90.17%	9.83%	89.52%	10.48%

Table S3. Calculated main electron configurations in the S_1 and T_1 states for NTO.

	S_1	T_1
	Transition component	Transition component
MAC-DPPN	H→L:99.61%; H-1→L+1:0.33%	H→L:96.99% H-1→L+1:1.46%
MAC-PN	H→L:98.64%; H-1→L+1:1.33%	H→L:98.45%; H-1→L+1:1.48%
PX-PN	H→L:98.56%; H-1→L+1:1.40%	H→L:98.21%; H-1→L+1:1.69%
PX-CNP	H→L:94.94%; H-1→L+1:5.01%	H→L:94.34%; H-1→L+1:5.01%

Table S4. The reorganization energies for S_0, S_1 states in S_0-S_1 transitions and T_1, S_1 states in S_1-T_1 transitions at low frequencies.

		$\lambda_{<200}(cm^{-1})$
S_0	MAC-DPPN	1245.76
	MAC-PN	753.53
	PX-PN	891.39
	PX-CNP	576.13
S_1	MAC-DPPN	3916.14
	MAC-PN	1384.11
	PX-PN	1332.20
	PX-CNP	983.80
T_1	MAC-DPPN	323.89
	MAC-PN	1344.71
	PX-PN	324.74
	PX-CNP	819.48
S_1	MAC-DPPN	233.79
	MAC-PN	1574.16
	PX-PN	311.25
	PX-CNP	852.85

Table S5. Basis test for vertical excitation energy (eV) of S1 state calculated with MPW1B95 functional.

	6-31G(d)	6-31G(d,p)	6-311G(d)
MCZ-DPPN	3.2847	3.2816	3.2564
MAC-PN	2.6837	2.6787	2.6756
PX-PN	2.4417	2.4374	2.4378

PX-CNP	1.9538	1.9502	1.9730

Table S6. Basis test for ΔE_{ST} (eV) of MAC-PN molecule with MPW1B95 functional.

MAC-PN	6-31G(d)	6-31G(d,p)	6-311G(d)	TZVP	def2-TZVP
ΔE_{ST}	0.060	0.060	0.054	0.053	0.052